Journal of Solid State Chemistry 182 (2009) 2036–2040

Contents lists available at ScienceDirect

Journal of Solid State Chemistry

journal homepage: www.elsevier.com/locate/jssc

Phase diagram features and solidification behaviour of $CoCu_2O_3$ at elevated oxygen pressure

N. Wizent *, L. Schramm, G. Behr, W. Löser, W. Gruner, A. Voß, B. Büchner, L. Schultz

IFW Dresden, Leibniz Institute for Solid State and Materials Research, Postfach 270116, D-01171 Dresden, Germany

ARTICLE INFO

Article history:
Received 3 March 2009
Received in revised form
28 April 2009
Accepted 30 April 2009
Available online 12 May 2009

Keywords:
Copper oxide
Phase diagram
Solidification

ABSTRACT

A unique behaviour of the phase $CoCu_2O_3$ was found both from CALPHAD calculations and directional solidification experiments. For elevated oxygen partial pressure the solidification mode changed from double-peritectic to a congruent melting behaviour with respect to the metals (Cu, Co) and to the oxygen content. This transition predicted by the phase diagram calculations was confirmed by microstructure and phase analyses of samples solidified at oxygen pressures up to 60 bar. A DTA analysis has verified basic features of the phase diagram at normal pressures.

1. Introduction

After the discovery of their high-T_c superconducting properties copper oxide compounds have attracted attention for many years [1]. The low dimensional spin ordering in cuprates in form of chains and ladders provides a unique possibility for basic research [2,3]. Cuprates do not only exhibit interesting physical phenomena. Thermodynamic aspects are of vital interest both for properties and preparation processes. Because copper can change its valence (Cu^{2+}, Cu^{1+}) the properties of cuprates can be designed by hole or electron doping. It turned out that elevated oxygen pressure promotes the presence of Cu^{3+} ions in the liquid phase and leads to considerable changes of phase equilibria in the binary Cu–O system [4]. It was shown that the melting temperature of CuO increases and the concentration difference between the melt and the CuO phase decreases with rising oxygen partial pressure. Accordingly, elevated oxygen pressure facilitated crystal growth of CuO by a floating zone (FZ) method with high growth rates up to 10 mm/h [5].

The Co–Cu–O system displays only one ternary phase $CoCu_2O_3$ and the binary terminal phases CuO, Cu_2O, CoO and Co_3O_4. $CoCu_2O_3$ is a spin ladder compound like $MgCu_2O_3$ and $CaCu_2O_3$ [6]. It possesses an orthorhombic *Pmmn* structure consisting of buckled ladders with an angle of 105° as shown in Fig. 1. The lattice parameters are $a \approx 9.408$ Å, $b \approx 3.980$ Å and $c \approx 3.198$ Å [6]. Under ambient pressures $CoCu_2O_3$ melts incongruently. Moreover, $CoCu_2O_3$ is a high-temperature phase, which decays into the binary oxides CuO+CoO below 1184 K [7]. In this work the effect of elevated oxygen partial pressure on the Co–Cu–O phase diagram and the solidification behaviour of $CoCu_2O_3$ were studied in order to provide a basis for the preparation of this (metastable) compound. Both, phase diagram calculations and droplet solidification experiments support a unique behaviour: The solidification mode of the $CoCu_2O_3$ phase changed from double-peritectic (with respect to the metal- and to the oxygen content) at normal pressure to a congruent melting at elevated oxygen pressure.

2. Experimental methods

The CuO powder (99.99%; Chempur) and Co_3O_4 powder (70% Co; Merck) were mixed, and sintered at 950–1000 °C for 24 h. After intermediate grinding, this procedure was repeated up to four times. The $CoCu_2O_3$ compound is not stable at room temperature. Therefore the sintered samples consisted of CuO+-CoO phases instead of single phase $CoCu_2O_3$. For solidification experiments rods of 6 mm in diameter were prepared. The powder was filled into latex tubes, pressed at 3500 bar hydrostatic pressure (EPSI, Belgium) and finally sintered 24 h at 1000 °C. The solidification experiments were performed in a laboratory type FZ crystal growth apparatus URN-2-ZM (MPEI, Moscow) with a vertical double ellipsoid optical configuration and a 5 kW air-cooled xenon lamp positioned near the focal point of the lower mirror. The cylindrical growth chamber is located near the focal point of the upper mirror (Fig. 2) [8–10]. For high pressure experiments a quartz cylinder with 14 mm wall thickness was utilized.

* Corresponding author. Fax: +49 351 4659 562.
E-mail address: N.Wizent@ifw-Dresden.de (N. Wizent).

0022-4596/$ - see front matter © 2009 Elsevier Inc. All rights reserved.
doi:10.1016/j.jssc.2009.04.035

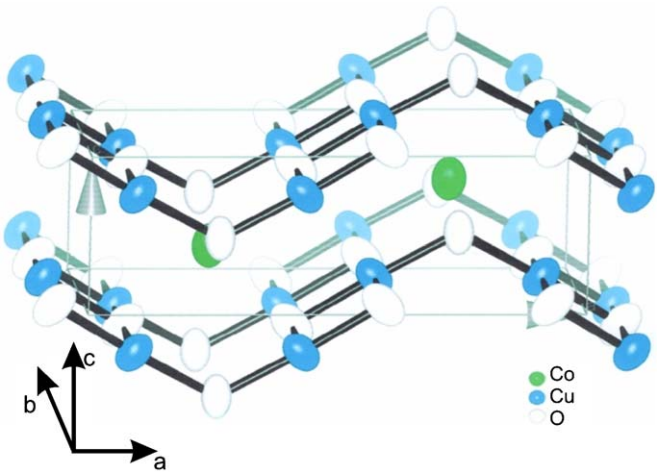

Fig. 1. Structure of $CoCu_2O_3$.

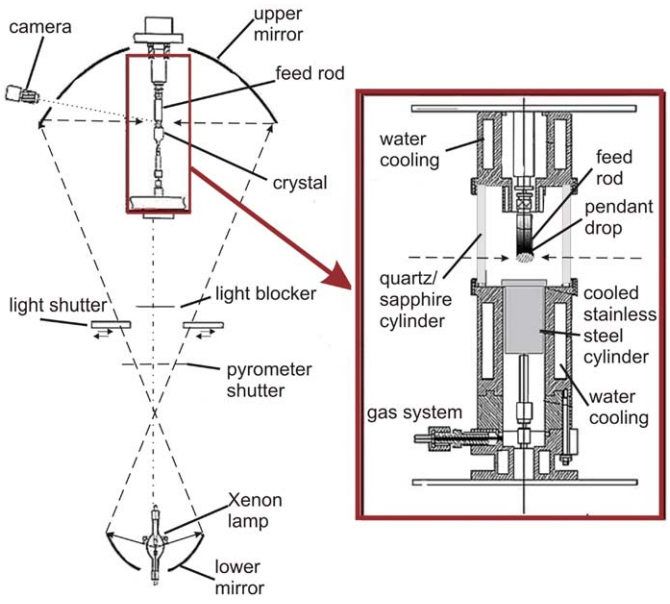

Fig. 2. Sketch of the vertical floating zone crystal growth apparatus with optical heating (left) and the modifications accomplished for the droplet solidification experiments (right).

Directional solidification experiments of suspended drops were performed (cf. Fig. 2). The tip of the feed rod was molten by increasing light intensity and homogenized with the gas atmosphere by keeping the suspending drop several minutes in the molten state. Then the feed rod was slowly moved upward with 5 mm/h. Thus, the droplet was gradually moved out of the focus and directionally solidified from the basis toward the tip. For any new experiment the tip of the feed rod was cut off to assure that no resolidified part from the last run remained. In addition to the directional solidification experiments droplets were molten, homogenized and then heated up until they fall down by gravity to be quenched in a water-cooled stainless steel mould. One unidirectional solidification experiment and three droplet quenching experiments were accomplished for each level of oxygen pressure (1, 30, and 60 bar).

The Co and Cu concentration of the as-solidified droplets were analysed by inductively coupled plasma-optical emission spectrometry (ICP-OES), and the oxygen content was using the a carrier gas hot extraction (CGHE) method. From the chemical analyses one can get an idea how melt composition and segregation effects depend on the oxygen pressure.

In order to identify the phase content and the microstructure the samples were cut and polished. The sections were investigated by optical microscopy (polarization microscope Axiovert 25 equipped with a Carl Zeiss digital camera) and the scanning electron microscope (SEM) Philips XL 30. Compositions of constituent phases were determined by electron probe microanalysis in the energy dispersive mode (EDX). A CuO single crystal was utilized as a standard for the determination of the oxygen content.

3. Results and discussion

3.1. Phase diagram calculations

The thermodynamic properties of the solid phases in the Co–Cu–O system have been analyzed by Zabdyr and Fabrichnaya [7]. Hence they determined the oxygen partial pressure vs. composition and calculated the Co–Cu–O phase diagram under ambient pressure. Here, parts of the ternary Co–Cu–O system were assessed for various oxygen pressures using the calculation of phase diagram (CALPHAD) technique. It is known from the Cu–O terminal system that the phase equilibria of the melt sensitively depend on the oxygen pressure [11,12]. Schramm et al. [4] have shown that the fit to the experimental data points of the pressure dependent CuO liquidus line can be considerably improved if Cu^{3+} ions are supposed as constituents of the ionic Cu–O liquid [9,13]. The model assumptions and the method of calculation for the ternary Co–Cu–O system follow the same line as described earlier in Ref. [4]. The liquid phase is represented by the two-sublattice model for ionic liquids. Similar to the binary Cu–O system the presence of Cu^{3+} ions in the liquid phase was presumed in this thermodynamic model. The $CoCu_2O_3$ phase was assumed to be a stoichiometric line compound although there is some solid solubility [7]. The Thermo-Calc program and the respective database, which rests on references [7,14], were used for the phase diagram calculation.

In Fig. 3 phase diagram projections to the CoO–CuO isopleths at three different oxygen partial pressures 1, 30, and 80 bar O_2 are compared. The CALPHAD calculations predict that the melting behaviour of $CoCu_2O_3$ changes considerably if the oxygen pressure increases. At 1 bar O_2 $CoCu_2O_3$ melts incongruently at 1159 °C. The projection to the CoO–CuO isopleths reflects this well known behaviour. The primary phase is CoO with a liquidus temperature $T_L = 1807$ °C. The $CoCu_2O_3$ phase is stable down to 915 °C where it decays into CoO+CuO. At 30 bar O_2 $CoCu_2O_3$ co-exists with a melt of the same Co and Cu content, which suggests congruent melting. However, from the isothermal Co–Cu–O phase diagram section 1 K above melting temperature, shown in Fig. 4a, it becomes clear that the oxygen content of $CoCu_2O_3$ and the co-existing melt still differ. The congruent melting behaviour is reached only at 80 bar O_2 where $CoCu_2O_3$ co-exists with a stoichiometric melt containing 50 at% O (Fig. 4b). In the CoO–CuO isopleths (Fig. 3c) the liquidus temperature of $CoCu_2O_3$ displays a distinct maximum at 1242 °C. By further increasing the oxygen pressure to 100 bar the melt can even be enriched with oxygen beyond 50 at% O. It is notified that the high oxygen pressure can also change the thermodynamic equilibria of the solid phases. The existence range of Co_3O_4 is extended to considerable higher temperatures as it becomes apparent from the sequence of Fig. 3a–c.

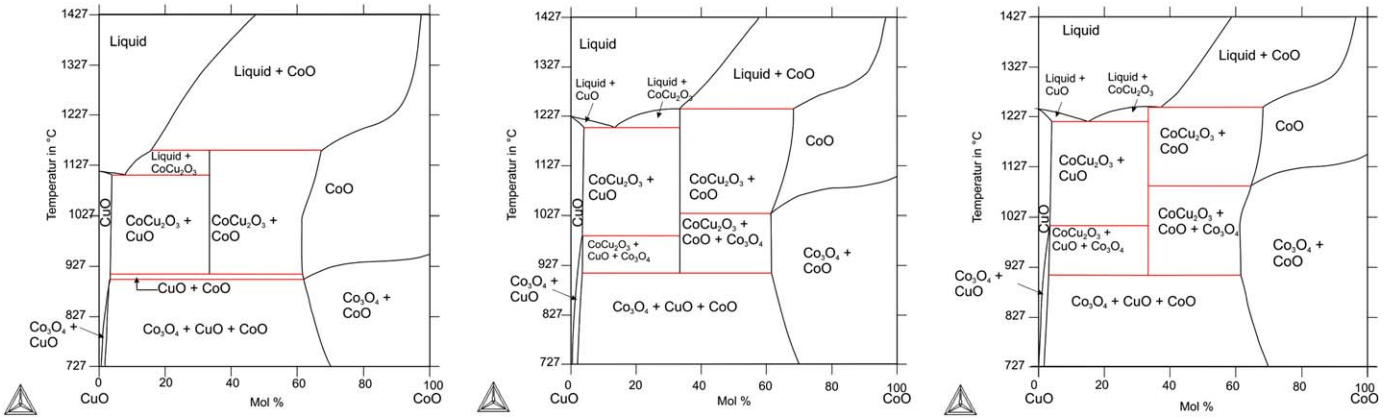

Fig. 3. Co–Cu–O phase diagram projections to the CoO–CuO isopleths for (a) 1 bar O_2, (b) 30 bar O_2 and (c) 80 bar O_2.

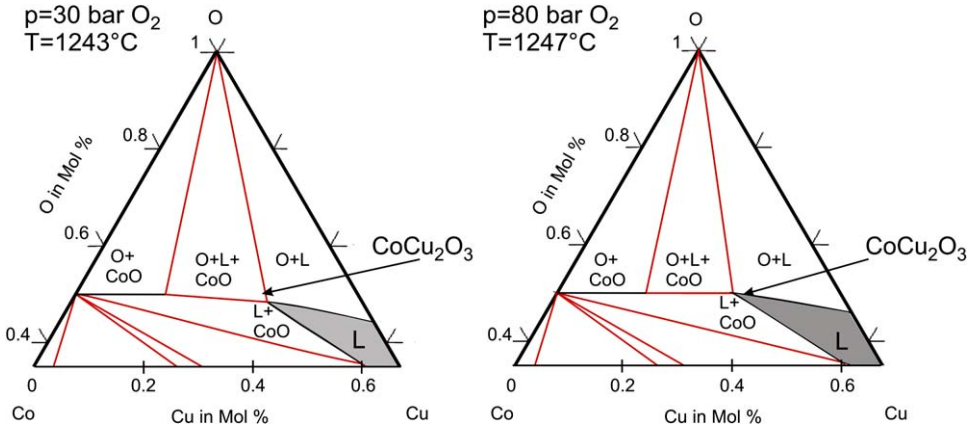

Fig. 4. Isothermal section (detail) of the ternary Co–Cu–O phase diagram 1 K above melting temperature of $CoCu_2O_3$ at (a) 30 bar O_2 (melting point: 1242 °C); (b) 80 bar O_2 (melting point: 1246 °C). The arrow is pointing to the composition of the $CoCu_2O_3$ phase.

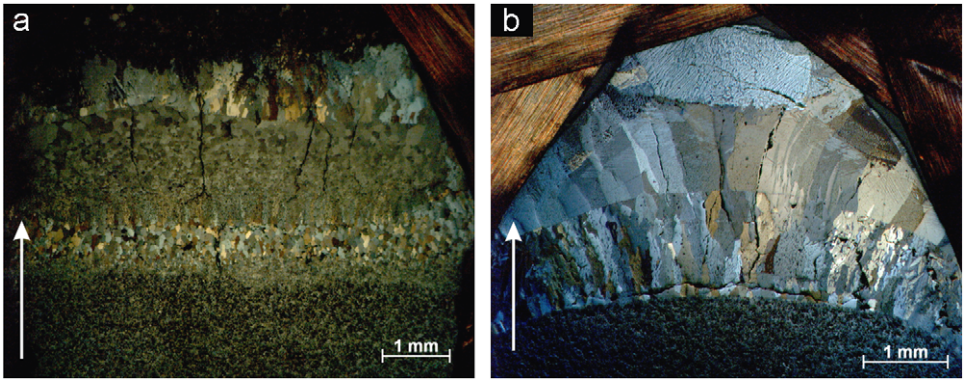

Fig. 5. Optical images of the grain structure of $CoCu_2O_3$ droplets directionally solidified from the bottom (feed rod) to the tip at different oxygen pressures (a) 1 bar, (b) 60 bar (arrow: growth direction).

3.2. Solidification experiments of Co–Cu–O melt droplets at various oxygen pressures

In order to verify the change of the melting behaviour predicted by the CALPHAD calculations we have performed unidirectional solidification and droplet quenching experiments. In Fig. 5 the microstructures of suspended droplets unidirectionally solidified from the bottom to the tip at two different oxygen pressures are compared. Both resolidified samples exhibit a layered microstructure, where the difference between the fine grained microstructure for solidification at 1 bar O_2 (Fig. 5a) and the columnar microstructure at 60 bar O_2 (Fig. 5b) becomes apparent from the optical image. In the latter case a successive coarsening of the columnar grains with proceeding growth is observed. In Fig. 5b close to the tip a lens-shaped region can be distinguished, which rather indicates a two-phase microstructure. The SEM image of the longitudinal section of a sample solidified at 1 bar O_2 shows a typical peritectic solidification microstructure (Fig. 6a). The solidification starts with the properitectic phase CoO (dark grey) from which the $CoCu_2O_3$ (light grey) is formed via the

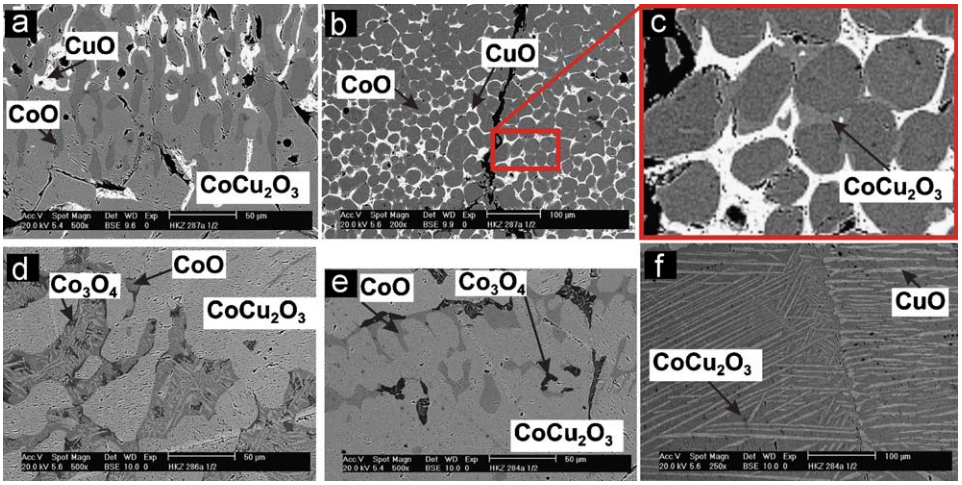

Fig. 6. SEM micrographs of $CoCu_2O_3$ droplets directionally solidified at various oxygen pressures: (a) longitudinal section (from bottom to top) at the start, (b) cross-section at the end for solidification at 1 bar O_2, (c) detail of Fig. 6b, (d) longitudinal section for solidification at 30 bar O_2, (e) longitudinal section at the start of solidification at 60 bar O_2 and (f) longitudinal section at the end of solidification at 60 bar O_2 ($CuO+CoCu_2O_3$ eutectic).

peritectic reaction $CoO+L \leftrightarrow CoCu_2O_3$. At the bottom of the droplet the initially formed CoO phase, which may exhibit a sizeable solid solubility of Cu according to Fig. 3, completely vanished. The reason is that this part of the sample was exposed to a long post-solidification heating during which the peritectic transformation was completed. At the end of the solidification three constituents CoO, $CoCu_2O_3$ and CuO (bright) appear. The CuO phase stems from the solidification of the residual melt, which forms a divorced eutectic CuO ($+CoCu_2O_3$). The typical features of the incomplete peritectic solidification become more apparent at the cross-section of the final part of solidification (Fig. 6b and c). The primarily formed CoO dendrites are surrounded by a rim of $CoCu_2O_3$ and separated by CuO in the interdendritic regions (see Fig. 6c).

At 30 bar O_2 the as-solidified microstructure is quite different. As shown in Fig. 6d the $CoCu_2O_3$ phase covers the main part of the sample section. Embedded are small patches which consist of a lamellar $CoCu_2O_3$+CoO microstructure and small grains of Co_3O_4 (dark). The volume fraction of those patches is reduced with advancing solidification, whereas CuO (one main microstructure constituent at 1 bar O_2) is completely absent. This obvious change of the solidification pathway is attributed to the phase diagram modification at elevated pressure. The $CoCu_2O_3$ phase crystallizes primarily instead of CoO. This can be explained by an increase of its melting temperature with rising oxygen pressure and the occurrence of a melting point maximum near the stoichiometric concentration (cf. Fig. 3b and c). The slightly Co-rich residual melt solidifies in form of the $CoCu_2O_3$+CoO eutectic. At normal pressure this solidification pathway toward a Co-rich residual melt is not allowed (cf. Fig. 3a). The composition of $CoCu_2O_3$, 16.8 ± 1 at% Co, 33.2 ± 1 at% Cu and 50.0 ± 0.5 at% O, determined by EDX, remains constant independent of the O_2 pressure. Whereas, the average eutectic composition, in agreement with the CALPHAD calculations, is shifted to higher cobalt contents with increasing oxygen pressure, from 6.5 at% CoO and 42.5 at% CuO at 1 bar O_2 to 12.5 at% Co and 37.8 at% Cu at 60 bar O_2. Within the eutectic patches (at 30 bar O_2) small grains of Co_3O_4 are detected. This can be attributed to the excess oxygen concentration in the melt which is further enhanced in the residual melt and finally leads to the Co_3O_4 precipitates from a supersaturated CoO phase. With proceeding solidification process copper is accumulated ahead of the solidification front. Near the tip of the suspended drop the Cu-rich melt finally solidifies as a lamellar $CuO+CoCu_2O_3$ eutectic (Fig. 6f).

The solidification microstructure at 60 bar O_2 (Fig. 6e) resembles that at 30 bar O_2. There is a high Co_3O_4 fraction, which shows that the melt is stronger enriched with oxygen in comparison to 30 bar O_2. Moreover, the predicted rise of the $3CoO + \frac{1}{2}O_2 \rightarrow Co_3O_4$ transformation temperature can accelerate the precipitation kinetics. This leads to coarse Co_3O_4 precipitates at 60 bar (Fig. 6e) in comparison to the sample solidified at 30 bar (Fig. 6d).

The solidification experiments confirm the enormous change of the melting behaviour of the $CoCu_2O_3$ phase at elevated oxygen pressure predicted by the phase diagram calculation (Figs. 3 and 4). More specifically, the solidification mode of $CoCu_2O_3$ is altered with respect to the fraction of metal ions (Cu/Co). Whereas, the phase equilibria are only marginally changed with respect to the oxygen content if the oxygen pressure increases (cf. Fig. 4). These features are rather unique and considerably differ from our previous studies of the Cu–O system [4], where the concentration difference of oxygen between the melt and the CuO phase decreased with increasing oxygen partial pressure.

Further evidence for the change of the solidification mode is provided by the chemical analysis of samples which were dropped down and quenched. At 30 and 60 bar O_2 the average composition of droplets agrees with the stoichiometric $CoCu_2O_3$ phase, which is consistent with the predicted congruent melting behaviour. At 1 bar O_2 the first droplet was Cu-rich, whereas the second one had a slightly higher Co-concentration. This rather suggests peritectic solidification where a mushy zone consisting of dendrites of the properitectic phase (CoO) and a Cu-rich melt is formed at the growth interface adjacent to the feed rod. Naturally, the dropped melt is Cu-rich because Co-rich dendrites remain (at least partially) at the feed. In the second run the remaining dendrites are remelted along with the feed rod and the overall composition of the melt is enriched in Co. Accordingly, the quenched sample exhibited a slightly higher Co concentration. Whereas composition fluctuations of the quenched droplets with respect to the (Cu/Co) fraction are only observed at 1 bar O_2, the oxygen content somewhat increased with increasing oxygen pressure (48 at% O at 1 bar compared with 50 at% O at 60 bar). This tendency is consistent to the calculated phase diagrams.

3.3. *Thermal stability of single phase $CoCu_2O_3$ specimen*

As confirmed by the solidification experiments $CoCu_2O_3$ can be retained as a metastable phase at room temperature [6]. The

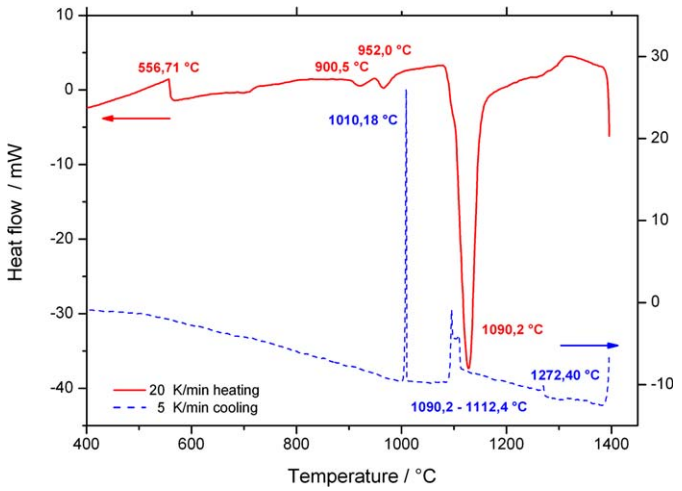

Fig. 7. DTA trace of $CoCu_2O_3$ at 1 bar O_2.

eutectoid decay into Co+Cu is suppressed if cooling is fast enough. Differential thermal analyses (DTA) up to 1400 °C with a heating rate of 20 K/min and a cooling rate of 5 K/min were performed on single phase $CoCu_2O_3$ samples at 1 bar O_2.

As shown in Fig. 7, on heating an exothermic reaction at 557 °C and two endothermic reactions at 900 and 952 °C, respectively, take place. The exothermic reaction at 557 °C can be attributed to the decomposition of $CoCu_2O_3$ to CoO+CuO. The phase fractions of samples from additional DTA runs (where heating was stopped at 650 °C with subsequent cooling with 20 K/min to room temperature) were checked by electron microprobe analysis. CoO and CuO precipitates were found in the $CoCu_2O_3$ matrix.

Two minor peaks on heating correspond to a release of oxygen according to a reaction $Co_3O_4 \rightarrow 3CoO + \frac{1}{2}O_2$ at 900 °C and the reformation of $CoCu_2O_3$, which becomes the stable phase above the eutectoid temperature $T_e = 952$ °C, from its transformation products. A detailed study of the solid state transformation mechanism is outside the scope of this paper.

The strong endothermic reaction can be identified as the onset of melting at the peritectic temperature $T_p = 1086$ °C. The experimentally determined value is below the calculated $T_p = 1159$ °C (Fig. 3a). The melting range extends up to the liquidus temperature $T_L = 1310$ °C in fair agreement with the calculated $T_L = 1327$ °C.

On cooling the primary crystallization of CoO occurs with a slight melt undercooling at 1272 °C. Further exothermic peaks between 1112 and 1090 °C can be attributed to the peritectic formation of $CoCu_2O_3$, which is not completed for moderate cooling. Therefore, the last sharp exothermic peak at 1010 °C is attributed to the eutectic reaction $L \rightarrow CoCu_2O_3$+CuO. No thermal event in the cooling trace can be identified for the slow solid state transformations. Electron microprobe analyses of the DTA sample verified CuO and $CoCu_2O_3$ as resulting phases. A thermogravimetric measurement shows a loss of mass due to the oxygen released, particularly at the melting point. During cooling the loss of mass could not be compensated, because the oxygen diffusion in the melt is too slow.

4. Conclusions

CALPHAD calculations for the Cu–Co–O system predicted a transition from incongruent melting toward congruent melting of the $CoCu_2O_3$ compound at elevated oxygen pressure. The change in solidification mode was experimentally confirmed by microstructure analysis of suspended droplets directionally solidified under high oxygen partial pressures up to 60 bar. The Cu–Co–O system is unique because high oxygen pressure leads to a modification of melting behaviour with respect to the fraction of metal ions (Cu/Co). The effect of elevated oxygen pressure on oxygen concentration of the phase equilibria is less pronounced. This is opposed too previous findings for the Cu–O binary system where the solidification of CuO strongly depends on the oxygen concentration of the melt at elevated oxygen pressure.

The melting temperatures experimentally determined by the DTA analysis at normal pressures are slightly below those of the CALPHAD calculations.

The experimentally found solidification behaviour provides fundamental information for the growth of $CoCu_2O_3$ single crystals. By using high oxygen pressure the growth could be facilitated and a faster growth velocity might be enabled where the phase decomposition during growth can be suppressed or at least reduced.

Acknowledgments

The authors thank S. Pichl, S. Müller-Litvanyi, J. Werner and U. Nitzsche for experimental and technical assistance and the DFG for financial support of the project Be1749/8.

References

[1] J.G. Bednorz, K.A. Müller, Z. Physik 64 (1986) 189–193.
[2] R.J. Cava, Science 247 (1990) 656–662.
[3] J.M. Tranquada, B.J. Sternlieb, J.D. Axe, Y. Nakamura, S. Uchida, Nature 375 (1995) 561–563.
[4] L. Schramm, G. Behr, W. Löser, K. Wetzig, J. Phase Equilibria Diffusion 26 (2005) 605–612.
[5] G. Behr, W. Löser, M.-O. Apostu, W. Gruner, M. Hücker, L. Schramm, D. Souptel, J. Werner, J. Cryst. Growth 40 (2005) 21–25.
[6] H. Müller-Buschbaum, A. Tomaszewska, Z. Kristallogr. 196 (1991) 1121–1127.
[7] L.A. Zabdyr, O.B. Fabrichnaya, J. Phase Equilibria Diffusion 23 (2002) 149–155.
[8] A.M. Balbashov, S.K. Egorov, J. Cryst. Growth 52 (1981) 498–504.
[9] G. Behr, W. Löser, D. Souptel, G. Fuchs, I. Mazilu, C. Cao, A. Köhler, L. Schultz, B. Büchner, J. Cryst. Growth 310 (2008) 2268–2276.
[10] D. Souptel, W. Löser, G. Behr, J. Cryst. Growth 300 (2007) 538–550.
[11] B. Hallstedt, D. Risold, L.J. Gauckler, J. Phase Equilibria 15 (1994) 483–499.
[12] A.V. Kosenko, G.A. Emel'chenko, J. Phase Equilibria 22 (2001) 12–19.
[13] B. Hallstedt, L.J. Gauckler, Comput. Coupling Phase Diagrams Thermochem. 27 (2003) 177–191.
[14] C. Landolt, A. Muan, J. Inorg. Nucl. Chem. 31 (1969) 1319–1326.